JTTEE5 13:561-569
DOI: 10.1361/10599630421497
1059-9630/$19.00 © ASM International

Peer Reviewed

Hot-Corrosion Behavior of Graded Thermal Barrier Coatings Formed by Plasma-Spraying Process

N. Mifune, Y. Harada, T. Doi, and R. Yamasaki

(Submitted November 4, 2003; in revised May 21, 2004)

The hot-corrosion behavior of thermal barrier coatings (TBCs) has been studied by comparing double-layer coatings and graded coatings. Two types of oxide ceramics, $2CaO{\cdot}SiO_2$-15mass%$CaO{\cdot}ZrO_2$ (C_2S-15CZ) and 8 mass% $Y_2O_3{\cdot}ZrO_2$ (8YSZ), with a bond coating of NiCrAlY, were applied to metallic substrates in this study. After hot-corrosion testing with V_2O_5-Na_2SO_4 corrosive ash for 3 h at 1273 K, the TBCs were investigated by visual inspection, a scanning electron microscope, x-ray diffraction, and electron probe microanalysis. The findings for the resulting coating of C_2S-15CZ reacted with V_2O_5 only where it was in direct contact with the corrosive ash. The affected area from the reaction was limited to the coating surface where V_2O_5 was present. The coating showed adequate hot-corrosion resistance against V_2O_5-Na_2SO_4 corrosive ash for 3 h at 1273 K. The findings for the 8YSZ coating were that Y_2O_3, the stabilizing component, particularly reacted with V_2O_5 and lost its function, which led to partial spalling of the coating. It was observed that the hot-corrosion resistance of the double-layer TBC was largely influenced by the performance of a corrosion-resistant NiCrAlY bond coat, which provided protection against corrosive components penetrating through the ceramic topcoat. Last, the graded coating degraded due to the oxidation of NiCrAlY particles that existed near the topcoat surface and affected the durability of the TBC.

Keywords calcium silicate, calcium zirconate, graded coating, hot corrosion, thermal barrier coating

1. Introduction

Industrial gas turbine (IGT) inlet temperatures have risen year by year. Increasing the operating temperature has proven to be the most effective method of directly improving the fuel efficiency of these power turbines. Due to the high combustion temperatures, cooling systems and materials with greater heat resistance and corrosion resistance have been studied extensively (Ref 1, 2). Thermal barrier coatings (TBCs) are widely used as thermal barriers to resist high temperatures and to protect the base metal from exposure to high temperatures, even when thin coatings are used (Ref 3). Thermal barrier coatings are also applied to critical hot sections of the IGT, namely, turbine blades, vanes, and combustion chambers (Ref 4). Most TBCs are sprayed with partially stabilized ZrO_2 and provide excellent performance with high-temperature stability and thermal-barrier protection. In addition to the heat resistance, TBCs are required to have hot-corrosion resistance with the use of low-quality fuels, which may contain corrosive constituents (Ref 2). The thermal-sprayed TBCs in this study consisted of graded and double-layer structures using a bond coat to improve the adhesion to the substrate and to assist in relieving the residual stress that may be produced during the thermal spray-coating process. However, in the double-layer coating, there is a difference in thermal expansion between the oxide ceramic topcoat and the metal bond coat, which can lead to spalling in high-temperature environments. To resolve this problem, a graded coating was designed to relieve thermal expansion mismatch stress (Ref 5-8).

The authors report here the results of a hot-corrosion study comparing TBCs. In this study, the topcoat ceramics materials for the TBCs were conventional 8 mass% $Y_2O_3{\cdot}ZrO_2$ (8YSZ) and $2CaO{\cdot}SiO_2$-15mass%$CaO{\cdot}ZrO_2$ (C_2S-15CZ, where C = CaO, S = SiO_2, and Z = ZrO_2), the latter being originally developed by Tocalo, Co. Ltd. (Kobe, Japan), and Nippon Steel Corp. (Tokyo, Japan) (Ref 9-11). A NiCrAlY bond coat was used for all of the TBCs. These ceramics and NiCrAlY coatings were applied by air plasma spraying.

2. Spraying of the Test Piece and Experimental Method

2.1 Thermal Spray Material

The TBCs were produced with a ceramic oxide topcoat using 8YSZ or C_2S-15CZ powders with a mean particle size of −44/+10 μm and a bond coat of Ni-22Cr-10Al-1Y (mass%) with a mean particle size of −44/+10 μm. Figure 1 shows the scanning electron microscope (SEM) images of C_2S-15CZ powder material produced with both fine particles of γC_2S (melting point: 2403 K) and CZ (melting point: 2618 K) by the spray-drying process and conventional 8YSZ (melting point: 2988 K) by the fused-and-crushed method.

2.2 Spraying Conditions

In this study, two oxide ceramics were air plasma sprayed to form test pieces of double-layer and graded coatings on type 304 austenitic stainless steel. The spraying conditions are shown in Table 1. The C_2S-15CZ material was sprayed with the same

N. Mifune, Y. Harada, T. Doi, and **R. Yamasaki,** TOCALO Co., Ltd., Kobe, Hyogo, Japan. Contact e-mail: y-migita@tocalo.co.jp.

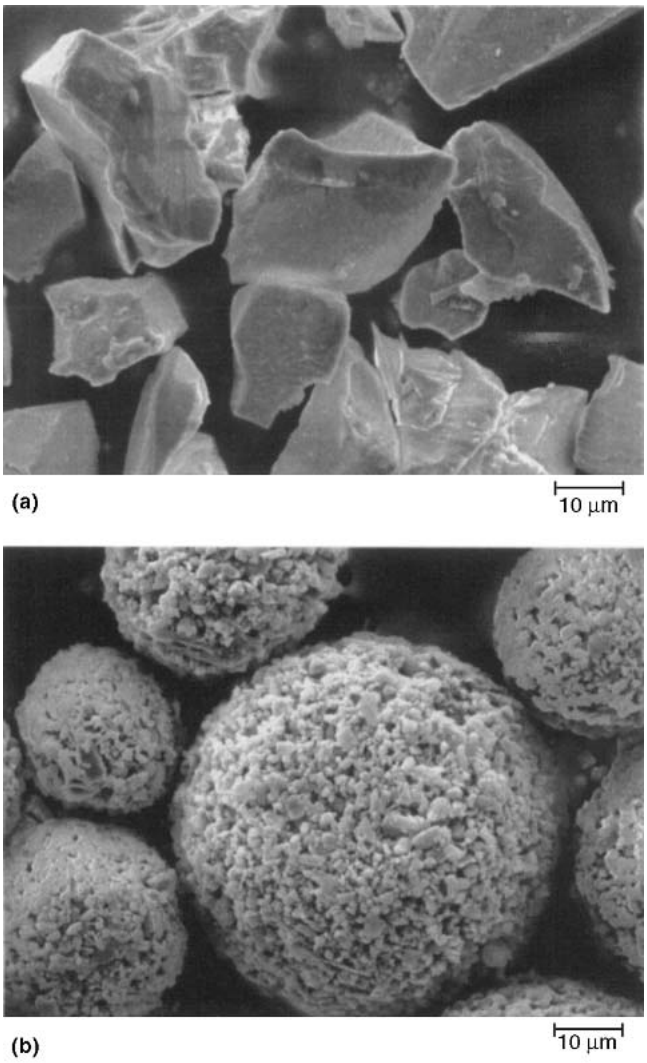

Fig. 1 Powder morphologies. (a) 8YSZ (fused and crushed powder). (b) C_2S-15CZ (agglomerated powder)

spray parameters as the 8YZ material to completely melt particles. The double-layer TBC was fabricated by spraying a 100 μm thick NiCrAlY bond coat and a 300 μm thick oxide ceramic top coat. The graded TBC coating consisted of intermediate layers with NiCrAlY alloy and oxide ceramics formed using four 100 μm thick layers; each layer increased in oxide ceramic content by 20 mass% toward the topcoat. A 100 μm thick oxide ceramic topcoat was sprayed on the intermediate layers (Table 1).

Scanning electron micrographs of the cross sections of the C_2S-15CZ/NiCrAlY coatings and the line analysis are shown in Fig. 2, which indicates the nickel component of the metal and the calcium component of the C_2S-15CZ ceramics.

The C_2S-15CZ topcoating exhibited many vertical microcracks within the single flattened ceramic particle, and no cracks through the topcoat. Figure 3 represents the x-ray diffraction (XRD) pattern of the C_2S-15CZ topcoating. The broad peak shown in the XRD signifies amorphouslike behavior within the microstructure. It has been previously reported by authors that the amorphouslike behavior and many fine microcracks are distinctive in the C_2S-15CZ coating (Ref 9-11).

Table 1 Thermal barrier coating materials and spray parameters

	Materials and spray parameters	
Item	**Composition, mass%**	**Thickness, μm**
Structure of TBC		
Double layer coating		
Bond coat	22Cr-10Al-1Y-balNi (NiCrAlY)	100
Topcoat	$8Y_2O_3{\cdot}ZrO_2$,C_2S-15CZ	300
Graded coating		
Bond coat	22Cr-10Al-1Y-balNi	100
Intermediate coat	80NiCrAl6-20 (oxide ceramic)	100
	60NiCrAlY-40 (oxide ceramic)	100
	40NiCrAlY-60 (oxide ceramic)	100
	20NiCrAlY-80 (oxide ceramic)	100
Topcoat	$8Y_2O_3{\cdot}ZrO_2$,C_2S-15CZ	100
	Spraying parameters	
Spray process	Atmospheric plasma spray	
Spray gun	Plasma technik type F4	
Plasma gas	Ar/H_2	
Power, kW	Topcoat (48), intermediate coat (46-47), bond coat (45)	
Spray distance, mm	120	

Table 2 Appearance of coated surface after hot corrosion test with corrosive ashes at 1273 K for 3 h

		Corrosive ashes, mass%	
Coating		**$85V_2O_5$-$15Na_2SO_4$**	**$15V_2O_5$-$85Na_2SO_4$**
8YSZ	Double layer	Spalling	Slightly light brown; no crack
	Graded coating	Significantly dark brown; no crack	Slightly light brown; no crack
C_2S-15CZ	Double layer	Whitened; no crack	Slightly whitened; no crack
	Graded coating	Whitened; no crack	Slightly whitened; no crack

2.3 Hot-Corrosion Test

The hot-corrosion properties of the TBC on the type 304 austenitic stainless steel substrate (100 × 50 × 5 mm) were tested. The test coupon was halved, and 10 mg/cm^2 corrosive ash was placed onto the center of each half in a 5 mm^2 area, as represented in Fig. 4. Two types of corrosive ash, namely, 85%V_2O_5-15Na_2SO_4 and 15V_2O_5-85$NaSO_4$ (mass%), were used for the test. Test pieces were placed into an air atmospheric electric furnace, which was heated up to 1273 K and held for 3 h. Subsequently, the samples were removed from the furnace and were cooled to room temperature.

The TBCs hot-corrosion behavior was evaluated by visual inspection, SEM micrographs of the coating cross sections, XRD, and electron probe microanalysis (EPMA).

3. Results and Discussion

3.1 Visual Inspection After the Hot-Corrosion Test

Table 2 shows the appearance of the double-layer coating and the graded coating after the hot-corrosion test using V_2O_5-

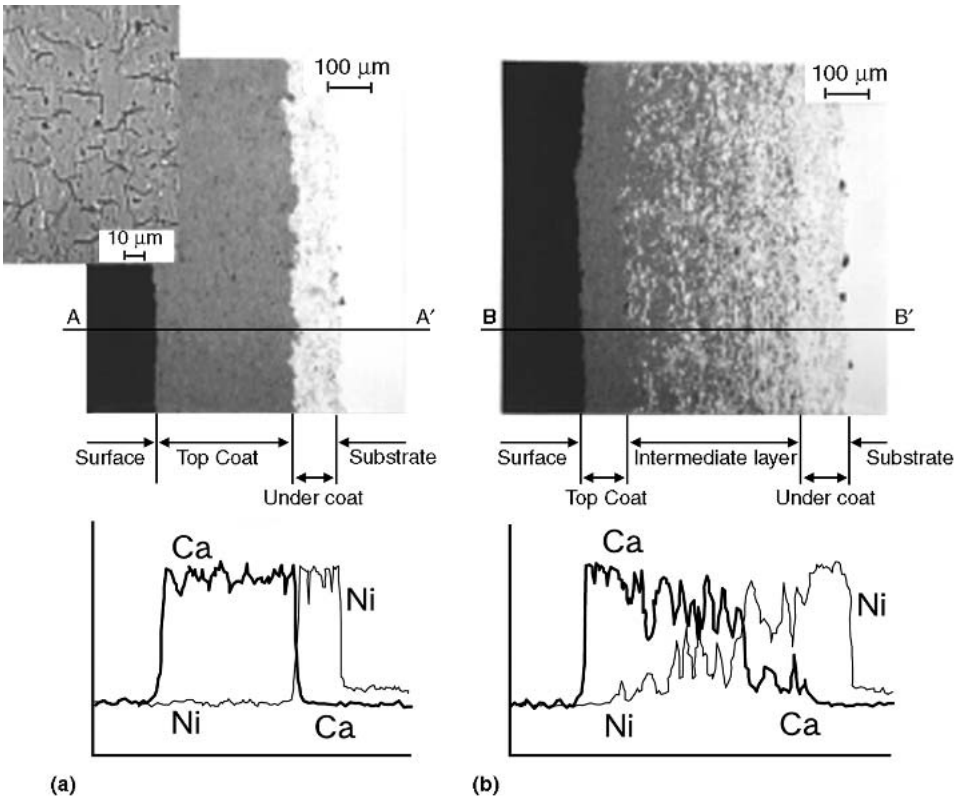

Fig. 2 SEM micrographs of the cross sections of as-sprayed C_2S-15CZ/NiCrAlY coatings and line analysis. (a) Double-layer coating. (b) Graded coating

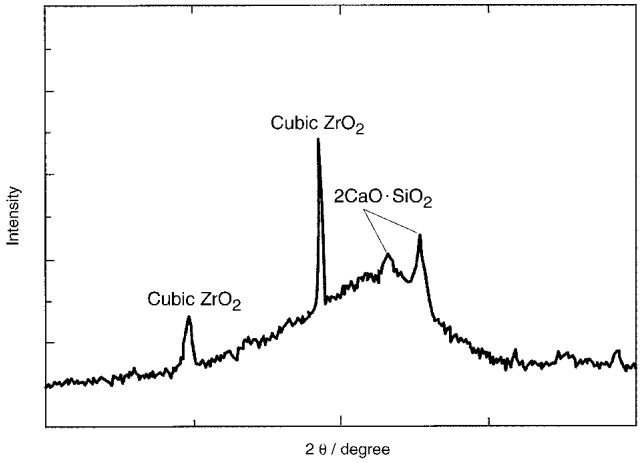

Fig. 3 XRD pattern of the C_2S-15CZ top coating

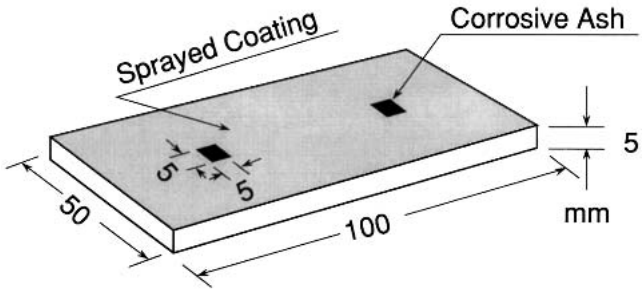

Fig. 4 Configuration of the TBC specimen

$NaSO_4$ corrosive ash for 3 h at 1273 K. The 8YSZ coating reacted slightly to the corrosive ash containing a small quantity of V_2O_5, and the result was a color change to light brown. In contrast, a significant color change to dark brown was observed on the 8YSZ coating when the corrosive ash was used with a high density of V_2O_5; especially for the 8YSZ double-layer TBC where the coating peeled away at the applied area of 85%V_2O_5-15%$NaSO_4$. As for the graded 8YSZ TBC, although the 8YSZ coating surface was corroded with 85%V_2O_5-15%Na_2SO_4 and the surface color was changed significantly to dark brown, no cracking or spalling was found.

A slight reaction to the corrosive ash containing V_2O_5 can be seen on the C_2S-15CZ coating, where the color of the reacted area changed to white. However, cracking and peeling were not visible on either the double-layer coating or the graded coating. The differences between the 8YSZ and the C_2S-15CZ coatings were observed to be significant, indicating that the latter coating material may have better corrosion resistance.

3.2 Cross-Sectional Observation After Hot-Corrosion Testing

Cross-sectional observation at the area applied with corrosive ash (15%V_2O_5-85%Na_2SO_4) revealed no defects on the 8YSZ double-layer coating. In the area with the 85%V_2O_5-15%Na_2SO_4 ash (Fig. 5), partial peeling and large cracks formed parallel to the substrate on the boundary between the 8YSZ topcoat and the bond coat. Figure 6 shows the cross-sectional SEM micrographs of the 8YSZ graded TBC after the hot-corrosion

test performed with 85%V_2O_5-15%Na_2SO_4 ash. The damage caused by the corrosive ash was restricted to the upper part of the intermediate layers and did not penetrate deeply.

Also, cross-sectional SEM and x-ray imaging of vanadium in the C_2S-15CZ-graded coating was observed (Fig. 7). The reaction between the topcoat and the corrosive ash was limited to the surface, with no reaction occurring within the coating.

3.3 Result of XRD

Many fine cracks and pores exist on the as-sprayed surfaces of the TBCs (Fig. 8). The authors believe that the corrosive ash easily penetrates these defects. However, although the pores reduce thermal conductivity, which improves the TBC function and provides stress relief, the pores and defects become the method of transport for the penetrating corrosive ash. X-ray diffraction on the TBC coatings after hot-corrosion testing with 85%V_2O_5-15%Na_2SO_4 ash was used to investigate the reaction behavior of TBC ceramics and corrosive ash (Table 3).

Due to the combustion process, it would be normal to find the presence of sulfur. Test results showed that no sulfur compound was found in the 8YSZ coating, but the authors did observe that Y_2O_3 reacted with the corrosive ash of V_2O_5 to form YVO_4 and $Y_8V_2O_{17}$. It was also observed that the corroded ZrO_2 existed in three kinds of crystal structures: cubic, tetragonal, and monoclinic. At temperatures between 1170 and 1370 K, the 8YSZ

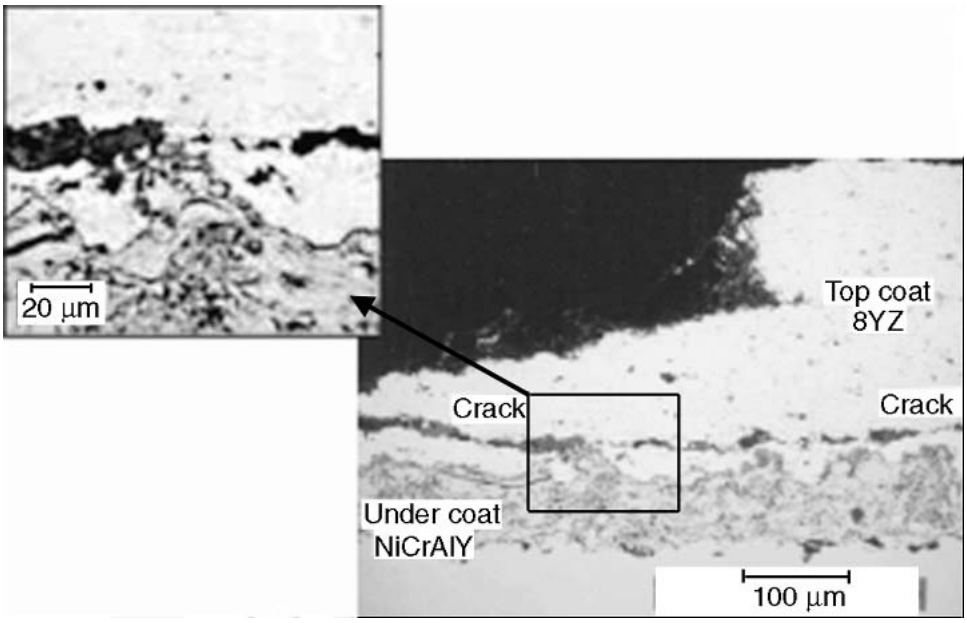

Fig. 5 SEM micrograph of a cross section of the 8YSZ double-layer coating after the hot-corrosion test with 85%V_2O_5-15%Na_2SO_4 ash at 1273 K for 3 h

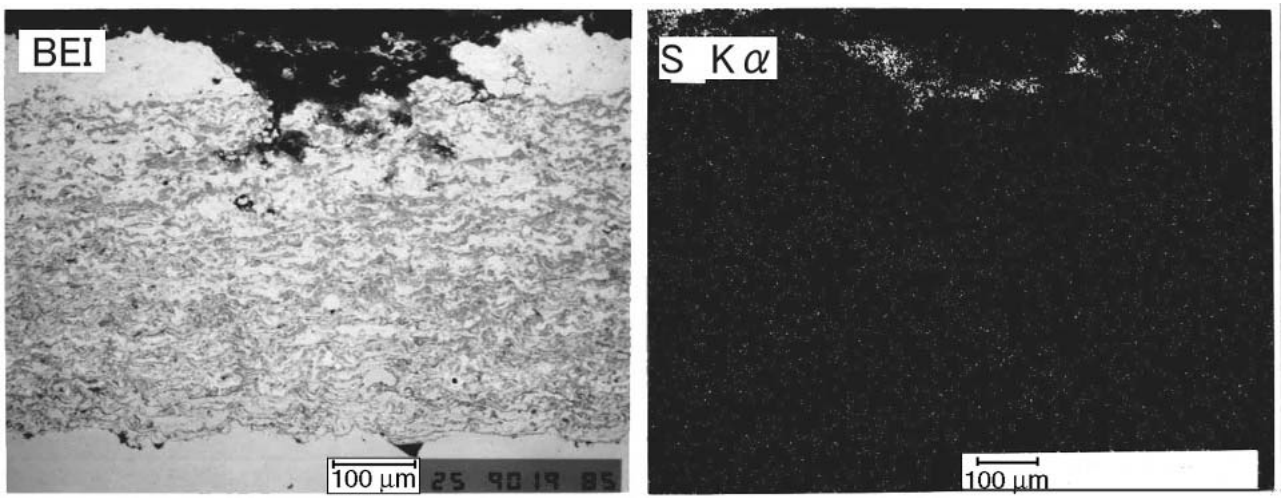

Fig. 6 SEM micrograph and x-ray image of a cross section of sulfur in the 8YSZ graded coating that was corroded with 85%V_2O_5-15%Na_2SO_4 at 1273 K for 3 h

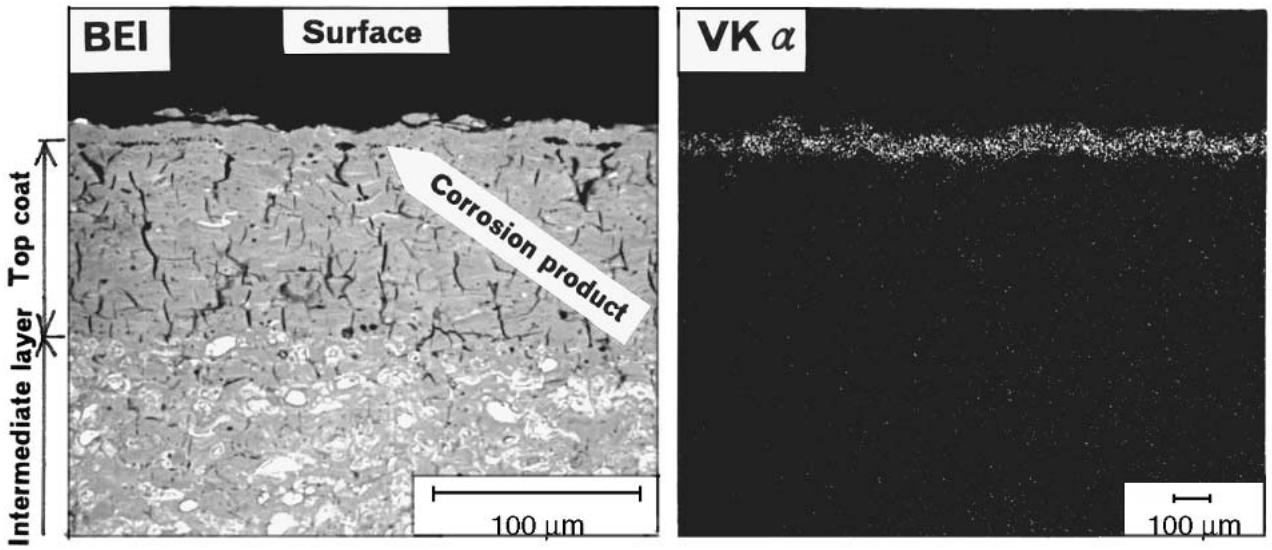

Fig. 7 Cross-sectional SEM micrograph and x-ray image of vanadium in the C_2S-15CZ-graded TBC after the hot-corrosion test with 85%V_2O_5-15%Na_2 corrosive ash at 1273 K for 3 h

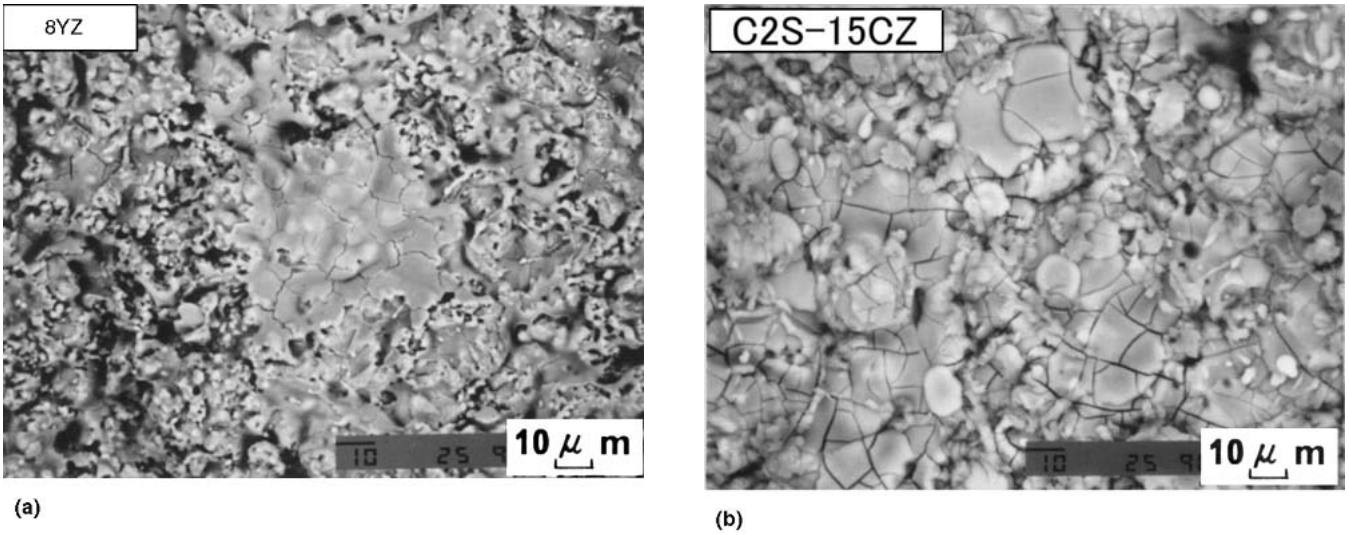

Fig. 8 Surface morphology of the as-sprayed 8YSZ and C_2S-15CZ coatings

coating with V_2O_5 lost its stabilizing component, Y_2O_3, according to the chemical reaction (Ref 12):

$$2ZrO_2 \cdot Y_2O_3 + V_2O_5 \rightarrow 2YVO_4 + ZrO_2 + ZrO_2 \cdot Y_2O_3$$

(ZrO_2 = monoclinic, $ZrO_2 \cdot Y_2O_3$ = tetragonal and cubic)

As a result, a large volume change due to the phase transformation between monoclinic and tetragonal structures took place, resulting in spalling (Ref 12). The peeling of the 8YSZ coating after the hot-corrosion test was attributed to this phase transformation.

Additionally, $2CaO \cdot V_2O_5$ and $CaSO_4$ were detected on the corroded area of the C_2S-15CZ coating, as shown in Table 3. Among these compounds, the vanadium-base corrosion substance was formed in a reaction between vanadium corrosive ash and the calcium component in the C_2S-15CZ coating at high temperatures:

$$2CaO \text{ (in } C_2S\text{-15CZ)} + V_2O_5 \rightarrow 2CaO \cdot V_2O_5$$

(melting point: 1051 K, Ref 13)

The heat resistance of the corroded C_2S-15CZ ceramics has probably been compromised, since the melting point is much lower than that of CaO (2845 K). It is, however, recognized that Y_2O_3 partially stabilized ZrO_2 involves the leaching of Y^{3+} when reacted with V_2O_5 (Ref 14):

$$Y_2O_3 + V_2O_5 \rightarrow 2Y^{3+} + 2VO_4^{3-}$$

Compared with Y^{3+} leaching, it is considered that the reaction between CaO and V_2O_5 is advantageous from the viewpoint of reaction kinetics.

Moreover, it was expected that the amorphous SiO_2 phase contained in the C_2S-15CZ coating decreased the corrosion (Ref 9). As for the Na_2SO_4 corrosive ash, this generates SO_x at high temperatures, which reacts with the calcium component. Consequently, stable $CaSO_4$ (melting point 1723 K) is formed and solidified, which aids in the corrosion resistance (Ref 11).

Table 3 X-ray diffraction results of thermal barrier coatings corroded with 85%V_2O_5-15%Na_2SO_4 at 1273 K for 3 h

Coating	Corrosion products	Coating structure
$8Y_2O_3$-ZrO_2	YVO_4,$Y_8V_2O_{17}$	c-ZrO_2, t-ZrO_2, m-ZrO_2
C_2S-15CZ	$2CaO{\cdot}V_2O_5$,$CaSO_4$	α-C_2S, $CaZrO_3$

Note: c, cubic; t, tetragonal; m, monoclinic

3.4 Structure of TBC and Hot-Corrosion Behavior of NiCrAlY

The cross-sectional SEM micrograph of the double-layer 8YSZ coating after the hot-corrosion test with 85%V_2O_5-15%$NaSO_4$ is shown in Fig. 5. The parallel crack is connected to the top of the NiCrAlY bond coat in the damaged area of the 8YSZ coating. The destruction of the 8YSZ coating may start in these regions. Considering these results, the large cracks on the

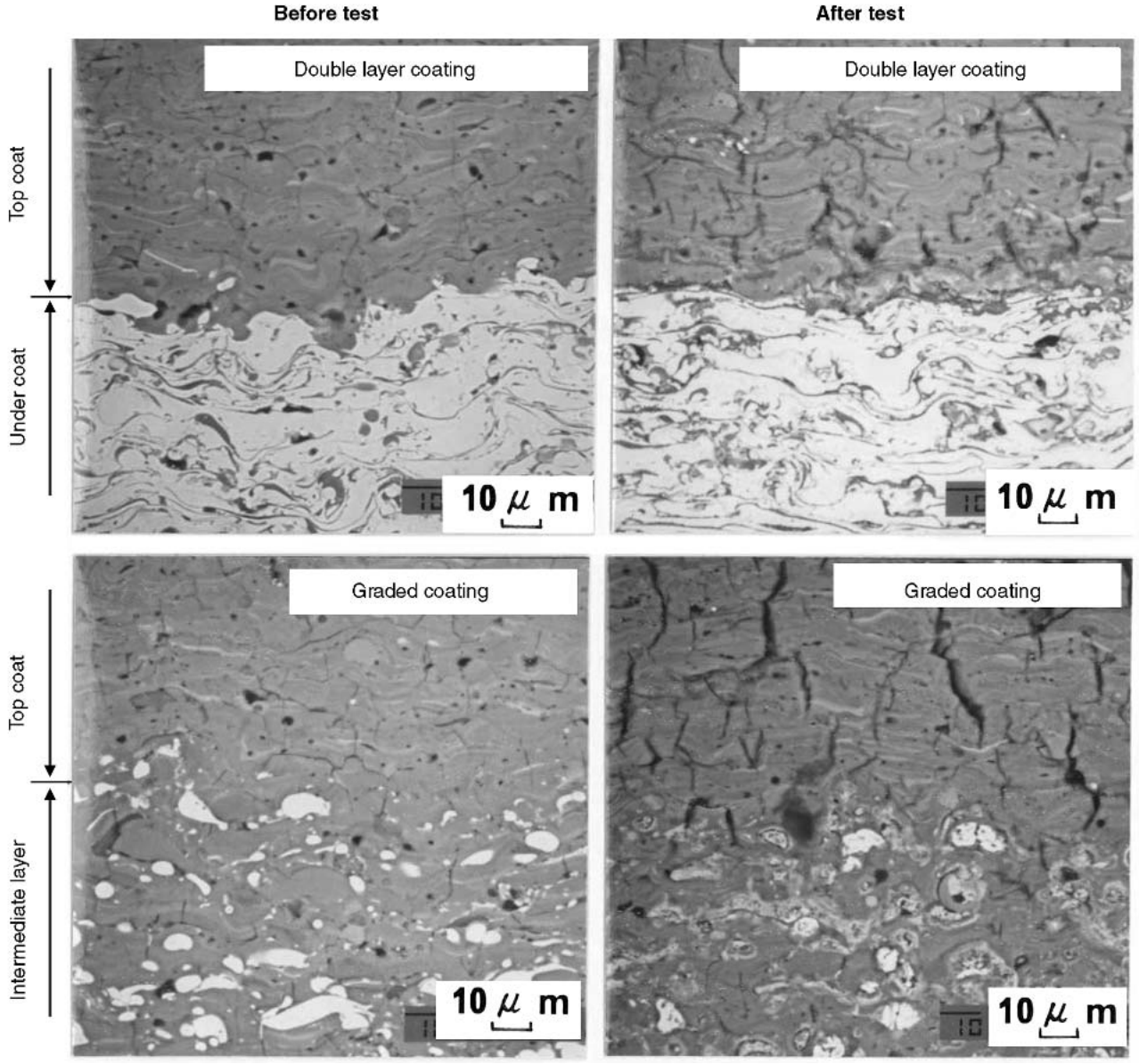

Fig. 9 Cross-sectional SEM of C_2S-15CZ/NiCrAlY contact region before and after the hot-corrosion test at 1273 K for 3 h with 85%V_2O_5-15%Na_2SO_4 corrosive ash

double-layer coating were caused not only by the difference in thermal expansion between the topcoat and the bond coat, but also by the reduction in corrosion resistance and strength of the bond coat at high temperatures. These findings indicate that the durability of a TBC depends on two factors: (a) using the optimum topcoat and bond coat materials and (b) the processing method that is used for depositing a thermal spray bond coat, since the bond coat had a great deal of influence on the damage to the TBC (Ref 15, 16).

Graded coatings can prevent the progression of cracks to intermediate layers because concentrations of thermal stresses are reduced due to the absence of a clear boundary between the bond coat and topcoat, as shown in Fig. 6 (Ref 17-20). As a result, the damage to graded TBC by hot corrosion was likely to occur in limited areas. The 3 h hot-corrosion test caused limited damage due to differences in thermal expansion rates between metal and oxide ceramics. The coefficient of thermal expansion of C_2S-15CZ, 8YSZ, and NiCrAlY coatings and type 304 stainless steel are 12.5×10^{-6}/K, 10.5×10^{-6}/K, 15×10^{-6}/K, and 18×10^{-6}/K, respectively (Ref 21).

The hot corrosion of NiCrAlY under the C_2S-15CZ coating is not macroscopically visible after the hot-corrosion test. However, the magnified observation by cross-sectional SEM micrographs shows the difference in the hot-corrosion behavior of NiCrAlY between the double-layer coating and the graded coating. The NiCrAlY corrosion damage in the double-layer coating started with contact with corrosive components (O_2,V_2O_5,Na_2SO_4) that flowed into the coating through pores within the topcoat. The NiCrAlY contained large amounts of chromium and aluminum with low energy of formation and yttrium, which improved the spalling resistance of the protective oxide coating by pegging (Ref 22). For these reasons, NiCrAlY coatings are generally regarded as a bond coat (Ref 23). Different features at the boundaries between the topcoat and the bond coat were observed, as shown in Fig. 9. This difference was observed in the double-layer coatings by EPMA in Fig. 10. Nickel is mainly visible, and a little aluminum is seen in the bond coat. The protective film of Al_2O_3 was not clearly distinguished. Large quantities of chromium were detected outside the boundary between the topcoat and the bond coat, where there was an overlap with the calcium-rich region of the topcoat. These results indicate that the protective oxide film of Al_2O_3 did not form sufficiently at the boundary area between the topcoat and the bond coat; that is, chromium seemed to have oxidized (Ref 24-26).

Figure 11 shows the EPMA micrographs of NiCrAlY particles included in a graded C_2S-15CZ coating after the hot-corrosion test. Aluminum exists with nickel and chromium in the element map, although significant formation of a protective Al_2O_3 film was not recognized. It is likely that NiCrAlY particles and C_2S-15CZ particles exist independently at the intermediate coat in the graded coating. Therefore, the independent NiCrAlY particles are oxidized at the surface by the corrosive component. The oxidized surface area of independent particles is much larger than that of the double-layer coating. Volume expansion rates of the NiCrAlY component due to oxidation are large; that is, Ni/NiO = 1.52, Cr/Cr_2O_3 = 1.99, and Al/Al_2O_3 = 1.28 (Ref 13). Volume expansion may cause the failure of the

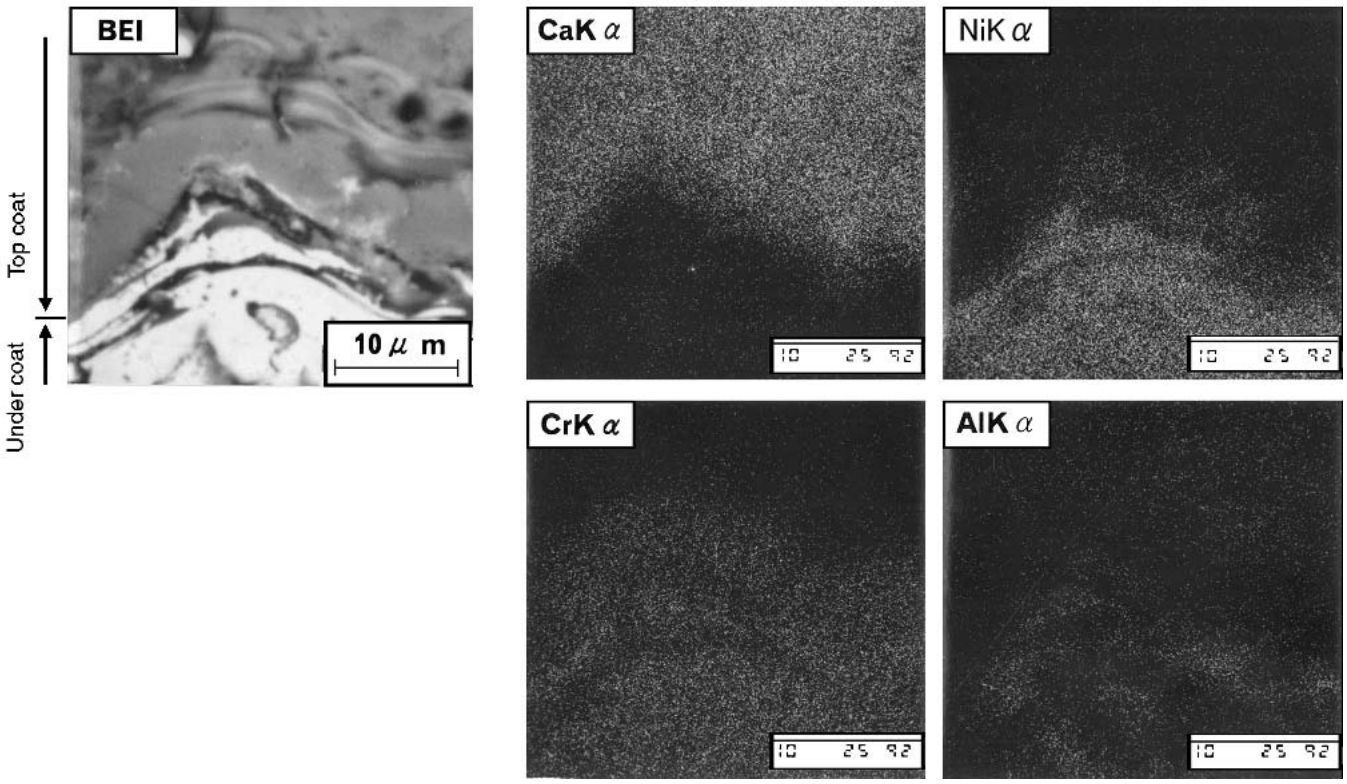

Fig. 10 EPMA image of the C_2S-15CZ/NiCrAlY contact region of the double-layer TBC after the hot-corrosion test at 1273 K for 3 h with 85%V_2O_5-15%Na_2SO_4 corrosive ash

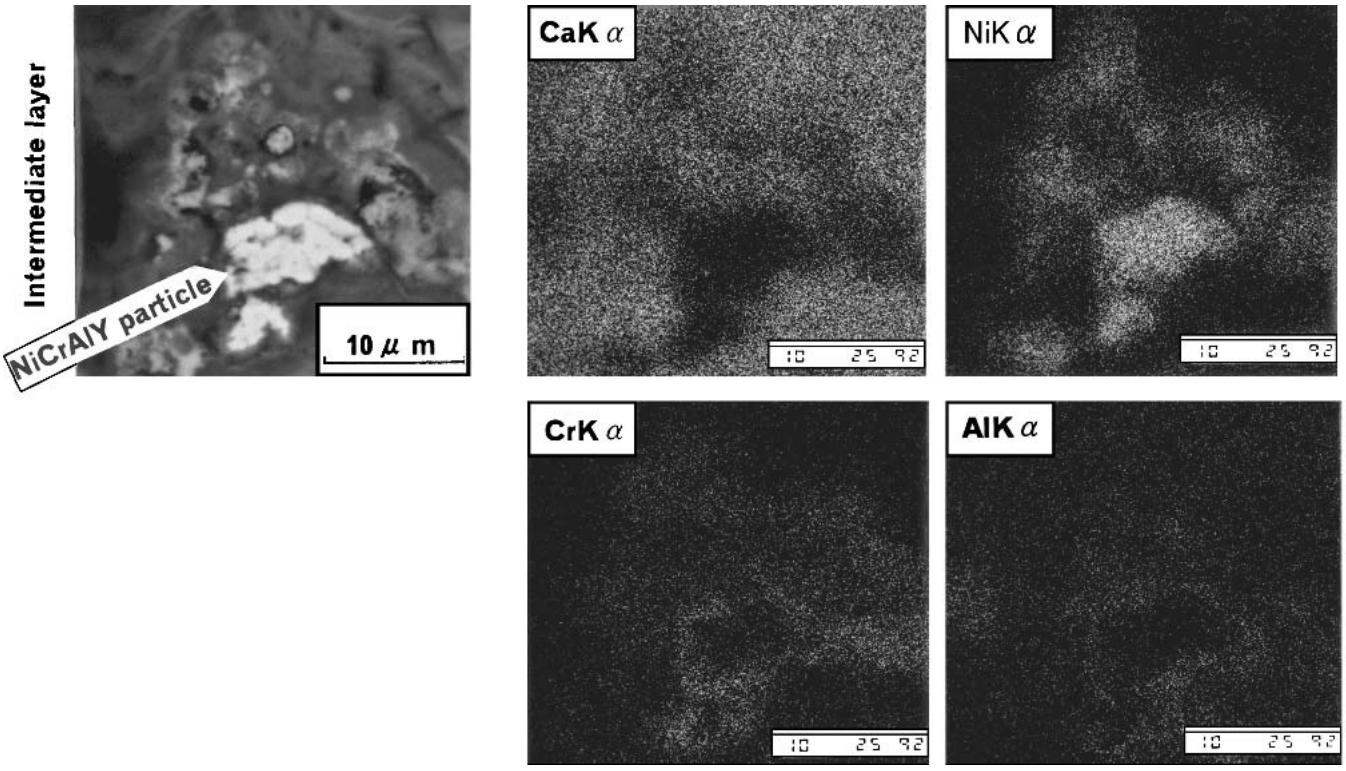

Fig. 11 EPMA image of the C_2S-15CZ/NiCrAlY contact region of the graded TBC after the hot-corrosion test at 1273 K for 3 h with 85%V_2O_5-15%Na_2SO_4 corrosive ash

TBC, originating at the particle boundary between C_2S-15CZ and NiCrAlY. Considering these situations, it is estimated that hot corrosion of the graded TBC begins with the oxidation of the NiCrAlY blended into the C_2S-15CZ, and the volume expansion causes destruction of the C_2S-15CZ boundary. This resulting phenomenon gradually proceeds to the inner layers.

4. Conclusions

The hot-corrosion behavior of a double-layer TBC and a graded TBC was examined by comparing the differences in the coating structure between C_2S-15CZ/NiCrAlY and 8YSZ/NiCrAlY while performing hot-corrosion tests at 1273 K for 3 h with 85%V_2O_5-15%Na_2SO_4 corrosive ash. The results are summarized:

- C_2S-15CZ, which forms the TBC topcoat, reacts with corrosive V_2O_5 and generates $2CaO \cdot V_2O_5$. It also forms $CaSO_4$ by reacting with Na_2SO_4. These reactions occur only at the contact regions with the corrosive component.
- The 8YSZ coating is corroded by V_2O_5 corrosive ash. The stabilizer, Y_2O_3, reacts with V_2O_5 and loses its function. This leads to the failure of the coating.
- With regard to the double-layer TBC, the hot-corrosion resistance was remarkably influenced by the performance of the NiCrAlY bond coat because the corrosive components penetrated through the ceramic topcoat.
- The durability of the graded TBC is affected by partial damage due to the oxidation of NiCrAlY particles in the graded area.

Acknowledgment

The authors are grateful to Dr. Robert Gansert of Hardface Alloys Inc. for reviewing a draft of this article.

References

1. H. Takeda, T. Suzuki, M. Ito, and Y, Takahashi, Gas Turbine Environments and Super Heat-Resistant Coatings, *J. Met. Finish. Soc. Jpn.,* Vol 38 (No. 12), 1987, p 586-591 (in Japanese)
2. N. Iwamoto, Development on Coatings for Gas Turbine, *Trans. Iron Steel Inst. Jpn.,* Vol 73, 1987, p 2187-2198 (in Japanese)
3. P.E. Hodge, S. Stecura, M.A. Gedwill, and I. Zaplatynsky, "Thermal Barrier Coatings: Burner Rig Hot Corrosion Test Results," NASA TM-79005, National Aeronautics and Space Administration, 1978
4. T. Suzuki and H. Takeda, Laser Surface Modification for Thermal Barrier Coatings, *Bull. Ceram. Soc. Jpn.,* Vol 25 (No. 10), 1990, p 964-969 (in Japanese)
5. T. Hashida, H. Takahashi, and K. Miyawaki, Evaluation of Thermal Shock Fracture of Functionally Gradient Materials, *J. Jpn. Soc. Powder Powder Metall.,* Vol 37 (No. 2), 1990, p 307-312 (in Japanese)
6. V. Pilous and J. Musil, Plasma Spraying of Graded Metal Ceramic Coatings, *Mater. Sci. Forum,* Vol 62 (No. 64), 1990, p 317-318
7. K. Kokini, J. DeJonge, S. Rangaraj, and B. Beardsley, Thermal Shock of Functionally Graded Thermal Barrier Coatings with Similar Thermal Resistance, *Surf. Coat. Technol.,* Vol 154 (No. 2-3), 2002, p 223-231
8. K.A. Khor, Y.W. Gu, and Z.L. Dong, Mechanical Behavior of Plasma Sprayed Functionally Graded YSZ/NiCrAlY Composite Coatings, *Surf. Coat. Technol.,* Vol 139 (No. 2-3), 2001, p 200-206
9. H. Nakahira, Y. Harada, N. Mifune, and T. Yagoro, High Temperature

Stabilities of $2CaO_2 \cdot SiO_2$-$CaO \cdot ZrO_2$ Thermal Barrier Coatings Formed by Plasma Spraying Process, *J. Gas Turbine Soc. Jpn.,* Vol 20 (No. 77), 1992, p 52-59 (in Japanese)
10. H. Nakahira, Y. Harada, N. Mifune, and T. Yagoro, Advanced Thermal Barrier Coatings Involving Efficient Vertical Microcracks, *J. Thermal Spray Technol.,* Vol 2, 1993, p 51-58
11. N. Mifune, Y. Harada, H. Taira, and S. Mishima, Field Evaluation of $2CaO \cdot SiO_2$-$CaO \cdot ZrO_2$ Thermal Barrier Coating on Gas Turbine Vanes, *Proceedings of 10th Thermal Spray Conference,* Thermal Spray: A United Forum for Scientific and Technological Advance, C.C. Berndt, Ed., American Society of Mechanical Engineering, 1997, p 299-303
12. P. Vincenzini, Zirconia Thermal Barrier Coatings for Engine Applications, *Ind. Ceram.,* Vol 10 (No. 3), 1990, p 113-126
13. *High Temperature Oxidation and High Temperature Corrosion of Metals,* The Japan Society of Corrosion Engineering/Maruzen Co., Ltd., Tokyo, Japan, 1982, p 97 (in Japanese)
14. A.S. Nagelberg, Destabilization of Yttria-Stabilized Zirconia Induced by Molten Sodium Vanadate-Sodium Sulfate Melts, *J. Electrochem. Soc.,* Vol 132 (No.10), 1985, p 2502-2507
15. Y. Mutoh, I. Sakamoto, and T. Nishimura, Failure Characteristics of Thermal-Cycled Zirconia Coatings, *J. Jpn. Thermal Spraying Soc.,* Vol 26 (No. 3), 1989, p 1140-1149 (in Japanese)
16. M. Yoshiba, K. Abe, T. Aranami, and Y. Harada, High-Temperature Oxidation and Hot Corrosion Behavior of Two Kinds of Thermal Barrier Coating Systems for Advanced Gas Turbines, *J. Thermal Spray Technol.,* Vol 5 (No. 3), 1996, p 259-268
17. Y. Tsunekawa, H. Harada, M. Okumiya, and I. Niimi, Heat Transfer in Thermal Barrier Coatings with Gradient Constituents Fabricated by Low Pressure Plasma Spraying, *J. Jpn. Inst. Met.,* Vol 54 (No. 11), 1990, p 1256-1260 (in Japanese)
18. T. Aihara, M. Kaji, and T. Igarashi, Numerical Analysis of Compositional Distribution Change in Functionally Gradient Materials, *J. Jpn. Inst. Metals,* Vol 54 (No. 7), 1990, p 758-763 (in Japanese)
19. D.S. Duvall and D.L. Ruckle, "Ceramic Thermal Barrier Coatings for Turbine Engine Components," 82-GT-322, American Society of Mechanical Engineers, 1982
20. F.C. Toriz, A.B. Thakker, and S.K. Gupta, "Thermal Barrier Coatings for Jet Engines," 88-GT-279, American Society of Mechanical Engineers, 1988
21. Y.J. Kim, T. Hashida, H. Takahashi, and K. Fujii, Evaluation of Mechanical Properties of Plasma Sprayed Zirconia/NiCrAlY Coating System by Means of Small Punch Testing Method, *J. Jpn. Thermal Spray. Soc.,* Vol 33 (No. 2), 1996, p 9-16 (in Japanese)
22. I.M. Allam, D.P. Whittle, and J. Stringer, The Oxidation Behavior of CoCrAl Systems Containing Active Element Additions, *Oxid. Met.,* Vol 12 (No. 1), 1978, p 35-66
23. Y. Itoh, Y. Ishiwata, and H. Kashiwaya, Microstructure and Thermal Conductivity of Thermal Barrier Coating, *J. Ceram. Soc. Jpn.,* Vol 98 (No. 6), 1990, p 561-566 (in Japanese)
24. M. Narumi, Z. Yu, H. Tarumi, and T. Narita, Oxidation Behavior of Plasma Sprayed CoNiCrAlY/YSZ Film at 1173 and 1273 K in Air, *Zairyou-to-Kankyo,* Vol 50, 2001, p 466-471 (in Japanese)
25. K. Ogawa, T. Masuda, and T. Shoji, Kinetics of Thermally Grown Oxide at Interface Between Thermal Barrier Coatings and MCrAlY Bond Coat, *Proceedings of International Thermal Spray Conference,* Thermal Spray 2001: New Surfaces for a New Millenium. C.C. Berndt, Ed., American Society of Mechanical Engineers, 2001, p 187-194
26. L. Lelait, S. Alperaine, and R. Mevrel, Alumina Scale Growth at Zirconia-MCrAlY Interface, *J. Mater. Sci.,* Vol 27, 1992, p 5-12